

# Energy-Efficient Driving in Connected Corridors via Minimum Principle Control: Vehicle-in-the-Loop Experimental Verification in Mixed Fleets

Tyler Ard, Longxiang Guo, Jihun Han, Yunyi Jia, Ardalan Vahidi, Dominik Karbowski

**Abstract**—Connected and automated vehicles (CAVs) can plan and actuate control that explicitly considers performance, system safety, and actuation constraints in a manner more efficient than their human-driven counterparts. In particular, eco-driving is enabled through connected exchange of information from signalized corridors that share their upcoming signal phase and timing (SPaT). This is accomplished in the proposed control approach, which follows first principles to plan a free-flow acceleration-optimal trajectory through green traffic light intervals by Pontryagin’s Minimum Principle in a feedback manner. Urban conditions are then imposed from exogenous traffic comprised of a mixture of human-driven vehicles (HVs) - as well as other CAVs. As such, safe disturbance compensation is achieved by implementing a model predictive controller (MPC) to anticipate and avoid collisions by issuing braking commands as necessary. The control strategy is experimentally vetted through vehicle-in-the-loop (VIL) of a prototype CAV that is embedded into a virtual traffic corridor realized through microsimulation. Up to 36% fuel savings are measured with the proposed control approach over a human-modelled driver, and it was found connectivity in the automation approach improved fuel economy by up to 26% over automation without. Additionally, the passive energy benefits realizable for human drivers when driving behind downstream CAVs are measured, showing up to 22% fuel savings in a HV when driving behind a small penetration of connectivity-enabled automated vehicles.

## I. INTRODUCTION

Cooperation in the longitudinal control of automated vehicles has soon realizable potentials for boosting energy and flow performance of real traffic in part due to connected technology [1]. Vectors of cooperation are primarily enabled through vehicle-to-infrastructure (V2I) and vehicle-to-vehicle (V2V) communication, which both leverage a plethora of efficient mobility strategies that arise via feedback and optimal control, and have been thoroughly evaluated through representative simulation [2]. Though, V2V-connected technologies have seen the majority share of the experimental validation to this point, even if V2I-enabled (or consequently I2V) technologies have perhaps the greater potential for environmental and mobility benefits between the two cases [3]. In part, V2I technology is practically challenged by the cost of required

Tyler Ard (trard@g.clemson.edu) and Ardalan Vahidi (avahidi@g.clemson.edu) are with the Department of Mechanical Engineering, Clemson University, Clemson, SC 29634, USA.

Longxiang Guo (longxig@g.clemson.edu) and Yunyi Jia (yunyij@g.clemson.edu) are with the Department of Automotive Engineering, Clemson University, Greenville, SC 29607, USA.

Jihun Han (jihun.han@anl.gov) and Dominik Karbowski (dkarbowski@anl.gov) are with the Energy Systems Division, Argonne National Lab, Lemont, IL 60439, USA.



Fig. 1: Viewpoint of driver in reality and in simulation during VIL testing of an urban corridor.

retrofitting of existing infrastructure, though recent initiatives have looked to address the technological barriers and create validation studies [4]. To address this, this manuscript details the experimental performance of a prototype CAV that performs eco-driving via optimally-guided motion planning given access to the SPaT of a V2I-connected corridor of traffic lights, and contributes experimental findings in the fuel economy benefits for both automated and nearby human drivers given access to connectivity in urban settings. This is accomplished by introducing a vehicle-in-the-loop experimental architecture, in which the physical ego vehicle interacts in real-time with microsimulated vehicles and intersections in a living virtual corridor. The experimental vehicle is depicted in Figure 1.

As connectivity and automation enters the market, significant performance benefits to an entire traffic scene are realizable under even partial connectivity and automation: while some CAVs have access to SPaT information and can directly optimize their motion, indirect performance benefits can extend to upstream traffic without said information by naturally responding to the motion of the CAV [5]. Typically, connected exchange of information allows the CAVs to anticipate downstream traffic patterns and drive in a traffic-stabilizing manner [6]. Such effects are well-studied through microsimulation of highway conditions: where increasing CAV penetrations in a merging scenario was shown to have a positive improvement on fleet fuel efficiency and traffic throughput [7], [8], and it was shown increasing CAV penetrations can reduce the number of braking events to suppress shockwaves that emerge in ordinary highway driving - which is directly beneficial to energy and fuel consumption [9], [10]. In urban settings, [11] shows a combined improvement to travel time and fuel economy in partial penetrations of CAVs equipped

with learned eco-driving policies that net-benefit the entire fleet. Similarly, [12] studies network-wide traffic benefits for both HVs and CAVs that are optimally guided to improve fuel economy, and [13] then considers impedance due to traffic build up behind red lights. In common to many of these studies, there exists a critical penetration of CAVs before performance benefits are consistently realizable - and usually requires a larger share of the market when increasing traffic volume demands.

Importantly, realizing benefits in connected communication does not necessarily require automation in both vehicles. Connected exchange of information from human driven vehicles in a traffic scene have also been used to boost traffic awareness in otherwise out-of-sight information, which enables more energy efficient driving strategies in CAVs. In [14], experimentation of several communication topologies of a string of connected and unconnected HVs and a CAV are employed to improve energy economy and traffic harmonization through mitigation of braking events, which is then further upscaled through microsimulation [15]. Improved traffic harmonization and dissipation of traffic shockwaves via predictive braking are shown in [16] for heavy duty trucks, finding a significant fuel economy improvement. In all studies, it is suggested that the largest benefits come from scenarios with long-range communication. Additionally, V2I-enabled eco-driving algorithms can benefit human drivers by displaying suggested driving speeds during intersection approach. Passenger vehicles were shown to, on average, improve fuel economy in [17] when eco-approach speeds were suggested to the driver through a vehicle dashboard interface, whereas [18] improve fuel economy of public transit buses by suggesting driving speeds to drivers.

Choice of control strategy is additionally important to realize performance benefits in CAVs. Earlier work in automated vehicle driving strategies developed predictive optimal control to anticipate surrounding vehicle and traffic light disturbances on urban roads to reduce reactionary braking - thereby improving fuel economy [19], [20]. In [21], a combination of V2V and V2I communication is used to efficiently navigate a corridor of traffic lights, in which the strategy explicitly considers effects of ego vehicle motion on upstream traffic; and in [22] a similar concept is extended using optimal control to further boost efficiency. Analytically-based controllers are shown for energy-efficient approach to signalized and non-signalized intersections in [23], [24]. When traffic light timings are not explicitly known, [25], [26] leverage probabilistic constraints in an optimal control problem for reasoning around uncertain signal timings for more robust eco-approach to intersections.

In prototyping CAVs which rely on control strategies that leverage other connected infrastructure and vehicles, much testing burden can be placed on experimentation due to high hardware and labor costs. Vehicle-in-the-loop (VIL) testing can instead focus on instrumentation and control for a small subset of physical vehicles, and upscale the traffic scenario through virtual microsimulation to populate other agents in the traffic scenario - which would otherwise require budgeting the still-expensive automation and connectivity hardware required to produce additional CAVs and supporting infrastructure.

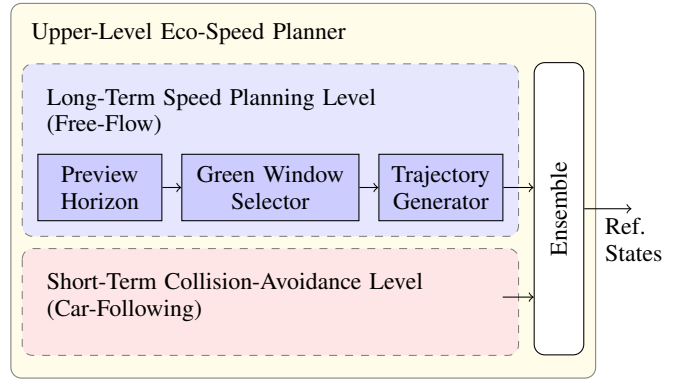


Fig. 2: Upper-level eco-speed planner structure.

Such VIL procedures additionally enable safe experimental testing: signal-less, autonomous intersections were first prototyped and implemented with an experimental CAV in a mixed reality fashion in [27], [28] - which can be otherwise dangerous to test if using multiple physical vehicles. Signalized intersections were studied in [29] with a suggestion-based controller that advises a human driver for the best intersection approach time in a virtual urban corridor, whereas [30] prototype a motion strategy in a variety of driving maneuvers to improve fuel economy inside of a corridor consisting fully of connected and automated vehicles (that leverages VIL testing capabilities developed in [31]). Eco-driving strategies in a mixed-traffic highway scenario were experimented on in [32] using VIL testing.

To this point, only a limited number of experimental studies involving CAVs equipped with V2I communication have been conducted: primarily, [33] novelly shows a 14% fuel benefit due to eco-driving a CAV informed with the SPaT of a connected intersection on a traffic-less road, whereas [34] show a 31% fuel benefit in a single intersection when introducing surrounding traffic, and [35] extend experimentation to multiple intersections in a single traffic corridor for again a 31% fuel benefit. As such, this paper aims to further study CAV capabilities in signalized traffic corridors. Multiple routes with varied traffic intersection positions and timings are considered - including those based on real data - and notably a wider variety of scenarios are tested by additionally introducing a partial penetration of CAVs in downstream traffic to assess their energy benefits on the experimental vehicle via smoothing. Additionally, this manuscript vets the effectiveness of an analytically-derived optimal controller via application of Pontryagin's Minimum Principle - which has not seen much experimental use in vehicle motion planning, despite the technique's effectiveness and low computational and hardware demands.

## II. UPPER-LEVEL ECO-SPEED PLANNER WITH PONTRYAGIN'S MINIMUM PRINCIPLE

The energy-efficient motion planning for the ego vehicle is performed in a two-level approach that is solved in a shrinking horizon fashion: the economic speed planning level formulates a long-term optimization problem that avoids unnecessary

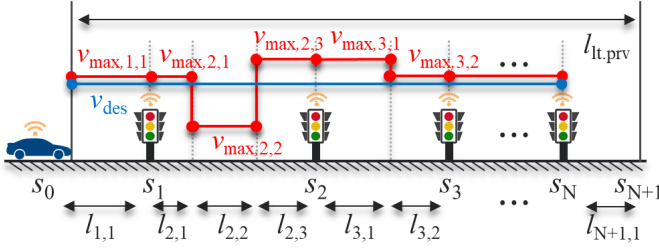


Fig. 3: Preview horizon diagram.

stops at intersections by utilizing connected traffic signal timing information, whereas the car-following level formulates a short-term optimization problem that maintains a desired time headway from the preceding vehicle. The two levels are fused through an ensemble module.

The motion planning problem is performed over a large route and contains non-convex interior constraints on the entering times through each intersection - both of which significantly increase the computational complexity. To deal with this, the optimal control problems are reformulated into bi-level optimizations, in which solutions to the newly-formed inner optimization have analytically-known explicit algebraic expressions via application of Pontryagin's Minimum Principle (PMP). The outer optimization is then efficiently, numerically solved on this condition. This approach enables control implementation even on computationally-restricted hardware, and resulted in sub-millisecond solution times for the considered scenarios.

Figure 2 illustrates the upper-level controller architecture. Commanded next-step vehicle velocity and acceleration then serve as reference states to be tracked using a low-level throttle and brake controller [32].

### A. Long-Term Speed Planning Level

At the long-term speed planning level, there are three modules to: set the problem boundary conditions according to the available preview horizon, decide the feasible green light windows according to available SPaT from in-horizon intersections, and generate energy-efficient vehicle trajectories.

1) *Preview Horizon*: The preview horizon is depicted in Figure 3, which connects  $N$  signalized intersections within range  $l_{lt,prv}$ . The end of the long-term preview horizon,  $s_{N+1}$ , then depends on whether a stop sign exists after the last connected traffic light. If a stop sign exists, then  $s_{N+1}$  is set as its position; otherwise, a virtual point  $s_{N+1} = s_N + \Delta s_{vp}$  is added. Correspondingly,  $N + 1$  segments divide up the road. As the speed limit trajectory is piecewise-constant, the  $i$ -th road segment can consist of  $n_i$  sub-segments. Accordingly, the maximum speed limit and length of the  $j$ -th sub-segment of the  $i$ -th road segment are defined as  $v_{max,i,j}$  and  $l_{i,j}$ , respectively.

2) *Green Window Selector*: In our previous work [36], the original green window selector module selects a series of green windows for each intersection that minimize an energy objective by path-search based on Dijkstra's algorithm. We simplify this energy-optimal path search problem into a

feasible path search problem so that additional computing resources are not required for any real-time implementation.

First, the *selected green windows* used to enter each intersection are computed to maintain the desired travel time, while also considering the known traffic light signal phase and timing (SPaT). The minimum and desired travel times for the  $i$ -th road segment are defined as

$$\xi_{min,i} = \sum_{j=1}^{n_i} \frac{l_{i,j}}{v_{max,i,j}}, \quad (1)$$

$$\xi_{des,i} = \frac{l_i}{v_{des}},$$

where  $v_{des}$  is the desired constant speed, and  $l_i = s_i - s_{i-1} = \sum_{j=1}^{n_i} l_{i,j}$ . Then, the desired entering-time at the  $i$ -th traffic light,  $t_{des,i}$ , can be sequentially computed starting from the current time  $t_{des,0} = t_0$ . Here, note that  $t_{des,i}$  is set to the next initial green phase timing if it falls within the non-green phases. For  $i = 1 \dots N+1$ ,

$$t_{des,i} = \begin{cases} t_{des,i-1} + \xi_{des,i} & \text{if } (\exists t_{gm,i}) \Phi_1(t_{gm,i}) \\ \{t_{gm,i} | \Phi_2(t_{gm,i})\} + \delta t_{gm,0} & \text{else} \end{cases} \quad (2)$$

with the two predicates

$$\Phi_1(x) = t_{des,i-1} + \xi_{des,i} \in [x + \delta t_{gm,0}, x + \Delta t_{gm} - \delta t_{gm,f}],$$

$$\Phi_2(x) = t_{des,i-1} + \xi_{des,i} \in [x - \Delta t_{cyc}, x],$$

and where  $t_{gm,i}$  is an initial green phase timing,  $\Delta t_{cyc}$  and  $\Delta t_{gm}$  are the durations of the entire traffic light cycle and green phase, respectively, and  $\delta t_{gm,0}$  and  $\delta t_{gm,f}$  are the safety time margins at the beginning and end of the green phase, respectively.

The minimum and maximum limits, denoted *feasible green windows*, are sequentially computed in a forward way (from the current time,  $t_{min,0} = t_0$ ) and a backward way (from the desired arrival time at the end of the preview horizon,  $t_{max,N+1} = t_{des,N+1}$ ), respectively:

$$t_{min,i} = \max(t_{min,i-1} + \xi_{min,i}, t_{des,i}) \text{ for } i = 1 \dots N,$$

$$t_{max,i} = \min(t_{max,i+1} - \xi_{min,i+1}, t_{des,i}) \text{ for } i = N \dots 1. \quad (3)$$

In a heuristic and computationally-efficient manner, this module generates a series of feasible green windows from desired entering-times for later use in energy-efficient trajectory generation of the CAV. This is illustrated further in Figure 4.

3) *Reference Trajectory Generator*: The long-term-horizon optimal control problem (OCP) is formulated assuming free-flow (FF) conditions and solved to generate the energy-efficient reference trajectory. To this end, interior-point constraints are first imposed by matching vehicle positions at each intersection's entering-time,  $t_{ent,i}$ , with  $s_i$ .

$$s(t_{ent,i}) = s_i, \quad i = 1 \dots N \quad (4)$$

Traffic-related parameters,  $\delta t_{des}$  and  $\delta t_{fea}$ , are then introduced respectively to promote entering intersections early and to tighten the feasible green windows to prevent entering intersections last-second. These parameters are calibrated to prevent long travel times within road segments that can cause unnecessary upstream traffic build-up. Compared from our

previous work [36] which introduced a traffic-related cost with a weighting factor that must be determined from batch simulation, these parameters are simplified to be intuitive and can be calibrated manually.

$$\begin{aligned} t_{\min,n,i} &= \max(t_{\text{des},i} - \delta t_{\text{des}}, t_{\min,i}), \\ t_{\max,n,i} &= \min(t_{\min,n,i} + \delta t_{\text{fea}}, t_{\max,i}). \end{aligned} \quad (5)$$

Finally, the long-term OCP is formulated by penalizing acceleration effort and using a double-integrator vehicle model.

$$\begin{aligned} \min_u \quad & J = \int_{t_0}^{t_f} 1/2 u^2 dt \\ \text{s.t.} \quad & \begin{cases} \dot{\mathbf{x}} = [x_2, a]^T = [x_2, u]^T \\ x_1(t_{\text{ent},i}) - s_i = 0, \quad i = 1 \dots N \\ t_{\min,n,i} \leq t_{\text{ent},i} \leq t_{\max,n,i}, \quad i = 1 \dots N \\ t_{\text{ent},i} - t_{\text{ent},i-1} \geq \xi_{\min,i}, \quad i = 1 \dots N \\ \mathbf{x}(t_0) = [s_0, v_0]^T \\ \mathbf{x}(t_f) = [s_f, v_f]^T \end{cases} \end{aligned} \quad (6)$$

where  $\mathbf{x} := [s, v]^T$ ,  $t_{\text{ent},0} = t_0$ , and boundary conditions are set by final time  $t_f = t_{\text{des},N+1}$ , final position  $s_f = s_{N+1}$ , and final velocity  $v_f$  as either 0 (a stop sign) or free.

The original OCP (6) is then reformulated into a bi-level optimization problem to facilitate analytical treatment. The inner OCP contains the trajectory optimization of the original OCP, while the outer optimization selects intersection entering-times that minimize the running cost of the inner OCP whilst satisfying its constraints.

$$\begin{aligned} \min_{\mathbf{t}_{\text{ent},i}, u^*} \quad & J = \sum_{i=1}^{N+1} \int_{t_{0,i}}^{t_{f,i}} 1/2 u^{*2} dt \\ \text{s.t.} \quad & \begin{cases} t_{\min,n,i} \leq t_{\text{ent},i} \leq t_{\max,n,i}, \quad i = 1 \dots N \\ t_{\text{ent},i} - t_{\text{ent},i-1} \geq \xi_{\min,i}, \quad i = 1 \dots N \\ u^* = \arg \min_u \int_{t_0}^{t_f} 1/2 u^2 dt \\ \text{s.t.} \quad \begin{cases} \dot{\mathbf{x}} = [x_2, u]^T \\ x_1(t_{\text{ent},i}) - s_i = 0, \quad i = 1 \dots N \\ \mathbf{x}(t_0) = [s_0, v_0]^T \\ \mathbf{x}(t_f) = [s_f, v_f]^T \end{cases} \end{cases} \end{cases} \end{aligned} \quad (7)$$

where

$$t_{0,i} = \begin{cases} t_0 & \text{if } i = 1 \\ t_{\text{ent},i-1} & \text{else,} \end{cases} \quad t_{f,i} = \begin{cases} t_f & \text{if } i = N + 1 \\ t_{\text{ent},i} & \text{else.} \end{cases}$$

The conventional, numerical way to solve the inner optimization could suffer from computational burdens. To this end, the optimal control policy for the inner OCP is shown to be a piece-wise linear function over  $(N+1)$  road segments through PMP analysis. The inner OCP is considered as a set of multiple unconstrained sub-OCPs with interior boundary conditions defined by  $\text{BC}_{\text{FF},i} = (v_{i-1}, v_i, l_i, \xi_i)$  and with  $\xi_i = t_{f,i} - t_{0,i}$ . These then provide the slope and intercept for each sub-OCP solution. Overall, the optimal entering speeds  $\mathbf{v}^* = [v_1^* \dots v_N^*]^T$  are given as

$$\mathbf{v}^* = \mathbf{A}^{-1} \mathbf{y}. \quad (8)$$

More details are shown in Appendices A and B. The cost of the outer optimization is expressed as a function of  $\mathbf{v}^*$  and  $\xi$ , where  $\xi = [\xi_1 \dots \xi_N]^T$ . The bi-level optimization problem is finally converted into a parametric optimization problem.

$$\begin{aligned} \min_{\xi} \quad & J = \sum_{i=1}^{N+1} J_i^* \\ \text{s.t.} \quad & \begin{cases} \mathbf{t}_{\min,n} \leq \mathbf{A}_{\text{ineq}} \xi \leq \mathbf{t}_{\max,n} \\ \xi \geq \xi_{\min} \\ \mathbf{y} = \mathbf{A} \mathbf{v}^* \end{cases} \end{aligned} \quad (9)$$

where  $J_i^* = 2(v_{i-1}^{*2} + v_{i-1}^* v_i^* + v_i^{*2}) \xi_i^{-1} - 6l_i(v_{i-1}^{*2} + v_i^{*2}) \xi_i^{-2} + 6l_i^2 \xi_i^{-3}$ , and  $\mathbf{A}_{\text{ineq}}$  is a lower unitriangular matrix.

The optimal travel times  $\xi^*$  are obtained by numerically solving the FF parametric optimization problem (9) - which additionally provides  $\mathbf{t}_{\text{ent}}^*$ . The equality constraint is used to compute  $\mathbf{v}^*$  as in (8), and the optimized boundary condition of the  $i$ -th road segment is then defined as  $\text{BC}_{\text{FF},i}^* = (s_{i-1}, v_{i-1}^*, t_{\text{ent},i-1}^*, s_i, v_i^*, t_{\text{ent},i}^*)$  for  $i = 1 \dots N + 1$ . The optimal acceleration trajectory of the  $i$ -th road segment is computed using  $\text{BC}_{\text{FF},i}^*$ , and each segment is stitched together to finalize the entire piece-wise linear function. At every time step, the long-term speed planning level provides the free-flow acceleration of the next step  $a_{\text{FF},n}$ .

## B. Short-Term Car-Following Level

The short-term car-following level focuses on car-following (CF) conditions that are not considered at the long-term speed planning level. The following CF-OCP is formulated to minimize acceleration effort while maintaining the desired inter-vehicle distance gap,  $s_d = v\tau_{\text{des}} + s_s$ . Here,  $\tau_{\text{des}}$  is the desired time gap, and  $s_s$  is a standstill safety distance.

$$\begin{aligned} \min_u \quad & J = \int_{t_0}^{t_{\text{st},\text{prv},f}} [(x_1 + x_2 \tau_{\text{des}} + s_s - s_p) + 1/2 w u^2] dt \\ & + \mu_1 (x_1(t_{\text{st},\text{prv},f}) - s_f)^2 + \mu_2 (x_2(t_{\text{st},\text{prv},f}) - v_f)^2 \\ \text{s.t.} \quad & \begin{cases} \dot{\mathbf{x}} = [x_2, a]^T = [x_2, u]^T \\ x_1 + x_2 \tau_{\text{des}} + s_s - s_p \leq 0 \\ \mathbf{x}(t_0) = [s_0, v_0]^T \end{cases} \end{aligned} \quad (10)$$

where  $t_{\text{st},\text{prv},f} = t_0 + t_{\text{st},\text{prv}}$ ,  $t_{\text{st},\text{prv}}$  is a short-term preview horizon,  $s_p$  is the position of the preceding vehicle, and  $(w, \mu_1, \mu_2)$  is a weighting factor set.

Similarly, the original CF-OCP is reformulated into a bi-level optimization problem to optimize the final conditions  $s_f$  and  $v_f$ .

$$\begin{aligned} \min_{s_f, v_f, u^*} \quad & J = \int_{t_0}^{t_{\text{st},\text{prv},f}} 1/2 u^{*2} dt \\ \text{s.t.} \quad & \begin{cases} s_f + v_f \tau_{\text{des}} + s_s - s_p(t_{\text{st},\text{prv},f}) = 0 \\ u^* = \arg \min_u \int_{t_0}^{t_{\text{st},\text{prv},f}} 1/2 u^2 dt \\ \text{s.t.} \quad \begin{cases} \dot{\mathbf{x}} = [x_2, u]^T \\ \mathbf{x}(t_0) = [s_0, v_0]^T \\ \mathbf{x}(t_{\text{st},\text{prv},f}) = [s_f, v_f]^T \end{cases} \end{cases} \end{cases} \end{aligned} \quad (11)$$

An analytical solution to the above inner unconstrained OCP can be derived in the same manner as the inner OCP in Eq. (7) and as shown in Figure 14. Then,  $J$  is expressed as a function of  $(s_f, v_f)$  following  $J_i^*$  as given in Eq. (9), where  $v_{i-1} = v_0$ ,  $v_i = v_f$ ,  $l_i = s_f - s_0$ , and  $\xi_i = t_{st,prv}$ . The bi-level CF-OCP (11) is reformulated into a constrained parametric optimization.

$$\begin{aligned} \min_{s_f, v_f} \quad & J = c_0 + c_1 s_f^2 + c_2 s_f + c_3 s_f v_f + c_4 v_f + c_5 v_f^2 \\ \text{s.t.} \quad & s_f + \tau_{des} v_f + s_s - s_p(t_{st,prv.f}) = 0 \end{aligned} \quad (12)$$

where  $c_0 = \frac{2v_0^2}{t_{st,prv}^2} + \frac{6v_0 s_0}{t_{st,prv}^2} + \frac{6s_0^2}{t_{st,prv}^3}$ ,  $c_1 = \frac{6}{t_{st,prv}^3}$ ,  $c_2 = -\frac{12s_0}{t_{st,prv}^3} - \frac{6v_0}{t_{st,prv}^2}$ ,  $c_3 = -\frac{6}{t_{st,prv}^2}$ ,  $c_4 = \frac{6s_0}{t_{st,prv}^2} + \frac{2v_0}{t_{st,prv}}$ , and  $c_5 = \frac{2}{t_{st,prv}}$ .

To predict  $s_p(t_{st,prv.f})$ , we assume that the preceding vehicle (PV) maintains its current acceleration  $a_{p,0}$  but limits its speed to its maximum ( $v_{des}$ ) or minimum (zero).

$$\begin{aligned} v_m &= \begin{cases} v_{des} & \text{if } a_{p,0} \geq 0 \\ 0 & \text{otherwise} \end{cases}, \\ t_m &= \min \left( t_{st,prv}, \max \left( 0, \frac{v_m - v_{p,0}}{a_{p,0}} \right) \right), \\ s_p(t_{st,prv.f}) &= s_{p,0} + v_{p,0} t_m + \frac{1}{2} a_{p,0} t_m^2 + v_m (t_{st,prv} - t_m) \end{aligned} \quad (13)$$

where  $s_{p,0}$  and  $v_{p,0}$  are the current PV position and speed, respectively.

The Karush-Kuhn-Tucker conditions are then applied to derive the analytical solutions as [37]

$$\begin{aligned} v_f^* &= -\frac{(2c_1 b_1 - c_3) b_0 + (c_2 b_1 - c_4)}{2(c_3 b_1 - c_5 - c_1 b_1^2)}, \\ s_f^* &= b_0 - b_1 v_f^*, \end{aligned} \quad (14)$$

where  $b_0 = s_p(t_{st,prv.f}) - s_s$  and  $b_1 = \tau_{des}$ . The optimal acceleration trajectory for the inner OCP in optimization (11) is computed using the optimized CF boundary conditions,  $BC_{CF}^* = (s_0, v_0, t_0, s_f^*, v_f^*, t_{st,prv.f})$ . At every time step, the short-term car-following level provides the collision-avoidance acceleration of the next step  $a_{CF,n}$ .

Finally, the ensemble module limits  $a_{FF,n}$  by  $a_{CF,n}$  to determine the final reference acceleration  $a_n$ .

$$a_n = \min(a_{FF,n}, a_{CF,n}) \quad (15)$$

Such a method can bring the energy benefits from long-sighted eco-driving as much as possible, while utilizing short-term car-following to ensure no rear-end collisions.

### III. TUNABLE PARAMETERS OF ECO-SPEED PLANNER

There are several parameters for the planner, and these parameters are pre-defined or tuned - and some can also be adjusted in real-time. In this section, key parameters are introduced to explain their impact on trajectory generation.

#### A. Preview Horizon Length

The long-term preview horizon for the speed planning level is distance-based - as its length  $l_{lt,prv}$  is determined by the number of connected traffic lights within V2I communication range. This distance-based preview horizon is converted to a time-based preview horizon via desired arrival time in the green window selector. On the other hand, the short-term preview horizon for the car-following level is time-based, and its length is limited to avoid collisions that might be caused by prediction mismatch from the realized PV trajectory. Here,  $t_{st,prv} = 3s$  was chosen. Note that an advanced PV prediction algorithm or intent sharing communication with a V2V-connected PV can increase  $t_{st,prv}$  such that a smoother trajectory can be generated.

As the ego vehicle travels, each of the preview horizons are to be updated. The long-term speed planning level uses a mix of a receding horizon and shrinking horizon approach: if there are connected traffic lights, the position of the last one defines the end of the preview horizon, and so the preview horizon is shrinking; otherwise, the preview horizon is receding with a fixed length. Here,  $\Delta_{s,vp} = 100m$  was set to enable eco-departure. On the other hand, the short-term car-following level always deploys the receding horizon methodology.

#### B. Desired Constant Speed

The final arrival time at the target destination is determined in the green window selector using parameter  $v_{des}$ . In general, the final arrival time can be shortened by increasing  $v_{des}$ , while it can also be influenced by catching green phases over multiple traffic signals regardless of  $v_{des}$ . In this paper,  $v_{des}$  is selected as a ratio to the constant maximum speed limit,  $r_{des} = v_{des}/v_{max,c}$ , where  $v_{max,c} = l_{lt,prv} / \sum_{i=1}^N \xi_{min,i}$ .

#### C. Traffic-Related Parameters

The reference trajectory generator provides the energy-optimal intersection entering-times, but these entering-times are additionally limited by the two calibration parameters,  $\delta t_{des}$  and  $\delta t_{fea}$ . With downstream traffic, short desired travel times can activate the car-following level frequently - which can then reduce the activity of the long-term speed planning level and reduce its energy benefits. On the other hand, long travel times can cause upstream traffic to miss available green phases or incentivize frequent lane changes. These two parameters can be intelligently adjusted using knowledge of the traffic.

#### D. Discussion

Figure 4 shows four different trajectories depending on the values ( $r_{des}, \delta t_{des}, \delta t_{fea}$ ). The first three are high-speed cases: in the case of upstream traffic, the values are set to (0.9, 5, 2) so that the ego vehicle can plan to pass through the intersections quickly. In the case of having both upstream and downstream traffic, the pair is set to (0.9, 1, 2) so that the ego vehicle can meet the original desired entering times for each intersection. In the case without traffic, the pair is set to (0.9, 5, 20) to loosen the entering-time limit constraint so that the ego vehicle can drive economically. Finally, the last case depicts a low

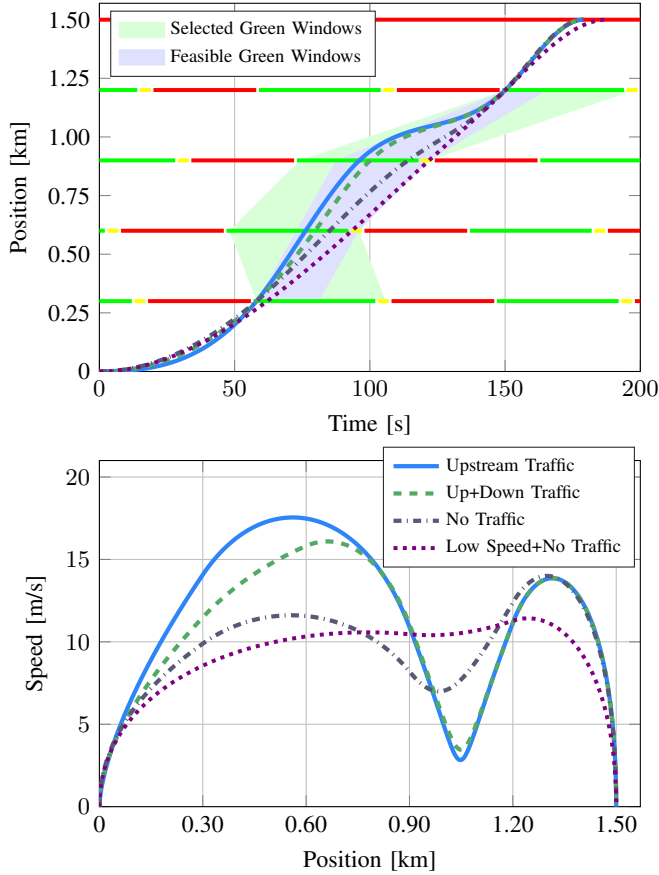


Fig. 4: Impact of parameters ( $r_{des}$ ,  $\delta t_{des}$ ,  $\delta t_{fea}$ ) with tunings for high speed cases of upstream, upstream and downstream, and no traffic; and for a low speed case with no traffic.

desired speed ratio of  $r_{des} = 0.7$  under traffic-less driving which enables smoother acceleration and relaxed final travel time.

#### IV. EXPERIMENTAL PROCEDURE

Testing was performed by driving the ego vehicle on a closed test track with on-board computing resources that simulate nearby human vehicles (HVs), connected and automated vehicles ((C)AVs), and intersections to virtually populate a surrounding traffic scene. Specifically, a single-lane corridor is considered with 14 vehicles downstream of the ego vehicle and 4 intersections used for creating urban driving conditions. An additional red-to-green traffic light is placed at the start of the route, and a stop sign is placed at the end to create boundary conditions for each trial. In the cases where downstream traffic contains a mixture of HVs and CAVs, a CAV is placed as the leading vehicle in the string and one is placed as the vehicle 3 downstream of the ego. The total available road length is 1.5 km at the testing facility, and a maximal vehicle velocity of 17.8 m/s is enforced for matching urban driving conditions. Small performance differences (2-3% difference in fuel economy) were measured depending on direction of travel at the testing facility due to road grade and weather conditions, so each experiment was repeated along each direction of the test track, for a total of 2 trials, and the results averaged. The

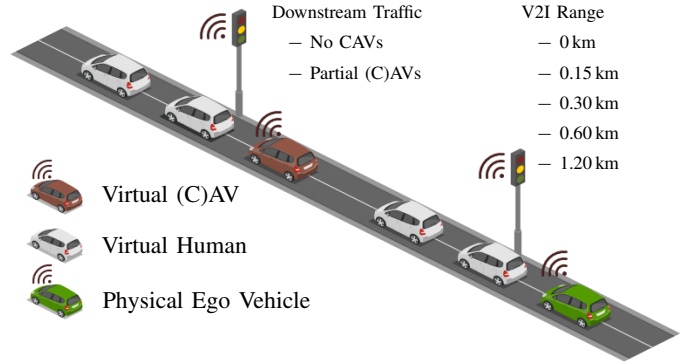


Fig. 5: Excerpt of scenarios considered. Diagram generated at icograms.com.

vehicle engine was kept warm between each test, and ambient air temperatures were within 10° F of each other between all tests.

Repeatability of the experiments is enforced by creating consistent boundary conditions between each trial of an experiment. A red-to-green traffic light is assigned at the beginning of the route and a stop sign is placed at the end of the track. The first traffic light starts red so that the string of vehicles can approach and come to a full stop. Then, fuel and travel time measurements are recorded in the interval between the first traffic light turning green and the ego vehicle travelling 99% of the distance to the end stop sign (the controllers brake at different comfort levels when approaching the stop sign). Figure 5 depicts a scaled diagram of the traffic scenario used in experiments.

The VIL experimental testing was performed for a multitude of scenarios. Namely, the downstream traffic composition was varied, the control strategy of the physical ego vehicle was varied, the maximal connectivity range of the considered V2I capability was varied, and the route that affects traffic light placement and timings was varied. The itemized list of the independent variables for experimental testing and their values are thus listed next.

- The downstream traffic composition was either: 1) all humans drivers and so *no CAVs*, or 2) mixed traffic with *partial (C)AVs* - where positions 1 and 11 in the string are CAVs.
- The control strategy of the ego vehicle was: 1) an *HV* using Wiedemann 99 model [38], 2) an unconnected *AV* using car-following MPC with reactionary braking for traffic light interactions [32], or 3) a *CAV* using the hierarchal eco-speed planning and car-following MPC approach of Section II.
- The maximal V2I connectivity range the intersections can broadcast at was considered for cases of 0.15 km, 0.30 km, 0.60 km, and 1.20 km. Additionally, a scenario in which there is *no V2I* connectivity available was considered.
- The designated route affected the traffic light position and timings, and was either: 1) a *synthetic* route that used a randomly chosen set of positions and SPaT of each light, or 2) the *Peachtree* street route extracted from the NGSIM

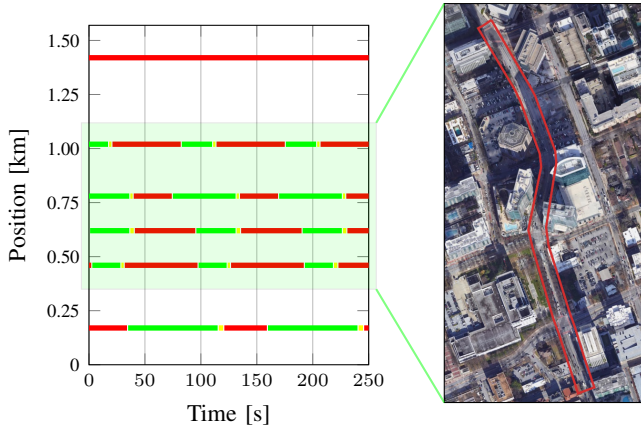


Fig. 6: Peachtree, ATL urban corridor. Signal position and green-amber-red timings shown on left, Google Earth view of corridor shown on right (outlined in red).



Fig. 7: Prototype CAV outfit with autonomy hardware stack used in VIL testing. Field experiments performed at ITIC in Greenville, SC.

dataset of midtown Atlanta, Georgia, USA.

Figure 6 depicts the Peachtree urban corridor traffic light timings as green, amber, and red intervals on a position versus time diagram. Additionally, the artificial first traffic light used to start each experimental trial and the stop sign placed at the end of the track are shown.

#### A. Vehicle Instrumentation

The experimental vehicle is a 2008 Mazda CX-7 that has been retrofit to add autonomous capabilities. The vehicle hardware stack includes a localization module, a communications and computation module, and a perception module. For localization, a Novatel PwrPak7-E1 dual-antenna RTK-GNSS with integrated IMU is used. For all onboard computation, a Dell mobile workstation with a quad-core 2.8 GHz Intel i7 processor and 16 GB of memory is used. The mobile workstation communicates with the sensors over ethernet through a Cisco 3560 network switch, and the clocks of the sensors are synchronized together using a TimeMachine 2000B Precision Time Protocol (PTP) server. For perception, a Velodyne VLP-16 LIDAR, an Ouster OS2-128 LIDAR, and two Mako G-

319C cameras are used. It should be noted that the VIL testing procedure provides ground truth sensors for vehicle motion planning against the virtual traffic scene, and so the perception hardware is only used as an autonomous safety feature against possible real obstacles at the testing facilities - such as stray wildlife.

Additionally, automatic vehicle actuation is achieved externally through steering wheel and pedal deflection robots using DC motors with a Roboteq MDC2460 motor driver. Experimental fuel measurements are as available in the field from OBD-II mass airflow readings that have been calibrated against fuel flow meter measurements. The vehicle used in testing is based on the experimental vehicle platform detailed previously in [32], and is depicted in Figure 7.

#### B. Vehicle Software

For vehicle software, socket-based communication with the microsimulation, sensor fusion, high-level motion planning, and low-level actuation control are performed through a ROS network. Position, orientation, velocity, and acceleration measurements from the guidance and inertial sensors are fused with a Kalman filter to reduce the effects of their noise on the control performance. The pedal deflection controller leverages a combined neural network-based feedforward and PID feedback control scheme to track the desired acceleration commanded from the motion planning controller of Section II. The lateral controller tracks a waypoint map - that matches the virtual microsimulated road network - using a pure pursuit scheme with look-ahead time and gain schedules for turning maneuvers of different curvatures. The low-level controller in this work executes at a frequency of 35 Hz on the mobile workstation, whereas the high-level controller executes at a frequency of 10 Hz (though can execute at a control frequency of over 100 Hz).

Real-time microsimulation of the surrounding virtual traffic scene is conducted using PTV Vissim. The Driver Model interface is used to program AV and CAV model behavior for select virtual traffic in microsimulation, while the Signal Control interface is used to set the fixed timings of the traffic lights in simulation and to communicate their SPaT to the physical ego CAV using a server-client protocol. Primarily, VIL is enabled using the Driving Simulator interface to extract distance and velocity readings of surrounding vehicles, as well as distance and current state of upcoming traffic lights, execute the microsimulation, communicate with the ego vehicle, and place the ego vehicle into the microsimulation scene in real-time [32].

## V. RESULTS AND DISCUSSION

For VIL experimentation, a control system on the prototype CAV is featured that processes communications from microsimulation, performs high-level motion planning for eco-driving, fuses and filters sensor information, and actuates external motors to control pedal deflection and steering angle. As such, control performance of the vehicle is first compared against a nominal simulation model of the vehicle to validate the efficacy of the deployed control strategy. Figure 8 depicts

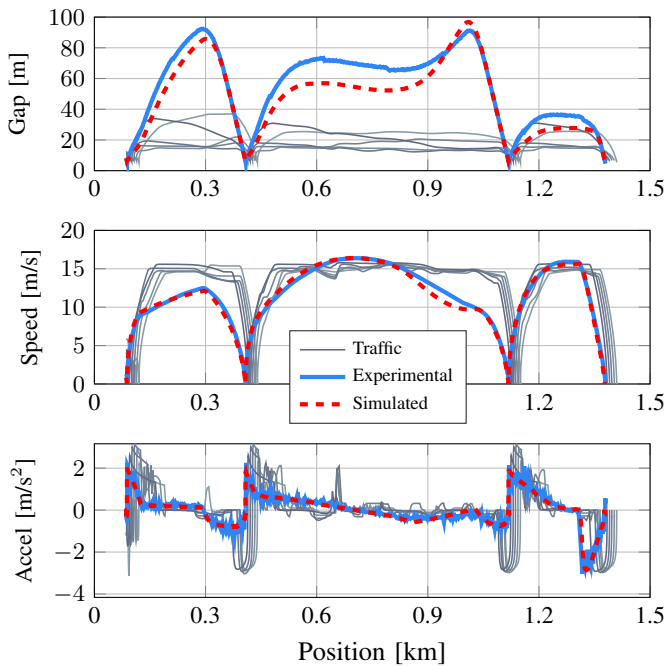


Fig. 8: Experimental versus simulated trajectories of the control approach on the real vehicle. Traffic is shown in black, with darker shades representing vehicles closer to the ego.

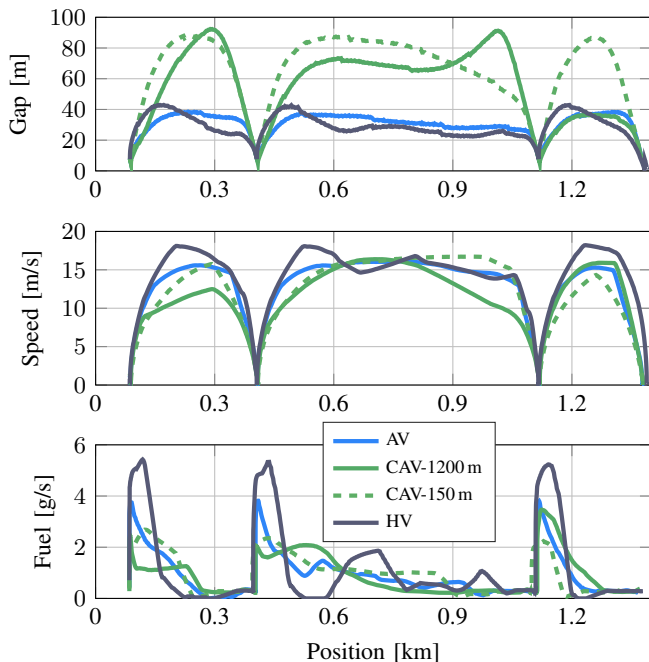


Fig. 9: Performance trajectories of the control approaches.

the realized gap, velocity, and acceleration trajectories of the ego vehicle in the same scenario from simulation and experimentation. Overall, the deployed physical vehicle control strategy strongly matches the predicted performance as from simulation.

Next, the different high-level controllers that perform motion planning are compared qualitatively in Figure 9 to ex-

amine how intersection approach and departure affected fuel performance differences. It can be seen that the CAV case with highest connectivity range cut speeding the most, which resulted in the least-incurred aerodynamic drag losses and lessened fuel expenditure. On the contrary, the HV featured the most aggressive driving patterns and reached the highest peak velocities, so fuel usage was particularly high when departing from intersections. Automation without connectivity cut unnecessary acceleration and braking for partial fuel savings and performed between the HV and CAV cases.

The overall VIL experimental fuel savings and travel time improvements are summarized in Figure 10, which reports savings for each case as compared to the HV baseline when driving in a traffic scene of all human drivers. In total, 62 experiments were run. It was found that increasing connectivity range improved fuel economy performance of both the ego vehicle when operating as a CAV and the ego vehicle when driving in mixed traffic scenarios - but was not necessarily automated or connected itself. Automation alone in the ego vehicle improved fuel economy between 13-15% for both routes chosen - and when the ego vehicle operated with connected information as well, fuel economy was improved between 19-36%. Travel time discrepancies were found to be within 3% of the HV baseline case in each trial (no more than 5 s), and negative travel time impact due to automation was primarily found in cases where the available connectivity range was limited (0.15 km case).

The presence of automation in a vehicle driving strategy has inherent energy benefits as compared to human driving behavior - due to smooth driving and reduction in unnecessary braking [32]. As such, we control for automation performance and examine energy benefits found due to the V2I-connected component of a CAV driving strategy over a native AV strategy. Figure 11 expresses the fuel and travel time improvements of the eco-driving approach in the CAV case with respect to the unconnected AV case. Here, the fundamental benefits of exploiting SPaT preview in eco-driving are compared to an approach that is limited to be only reactionary to traffic lights. Overall, including SPaT preview in the motion planning of a CAV improved fuel economy between 4-26% over the preview-less AV case. When V2I connectivity range was at least 300 m (far enough to guarantee range of at least 1 intersection when travelling throughout the route), fuel improvement increased to between 13-26%. Travel time impact was limited to be within 3% of the AV case in each trial (no more than 5 s).

For the scenarios used, there was not a significant performance difference for the ego vehicle when driving in either the partial AV case versus no AV case - largely because the downstream AV penetration rate was too lean to significantly attenuate traffic-induced speed fluctuations that require the ego vehicle to brake. However, with the same number of downstream CAVs in the network, two effects can be noted: 1) if the ego vehicle is operating as an HV, downstream CAVs provide a significant fuel benefit by indirectly improving ego traffic light interactions, and 2) if the ego vehicle is operating as a CAV with limited connectivity range, presence of downstream CAVs can further improve fuel economy - as



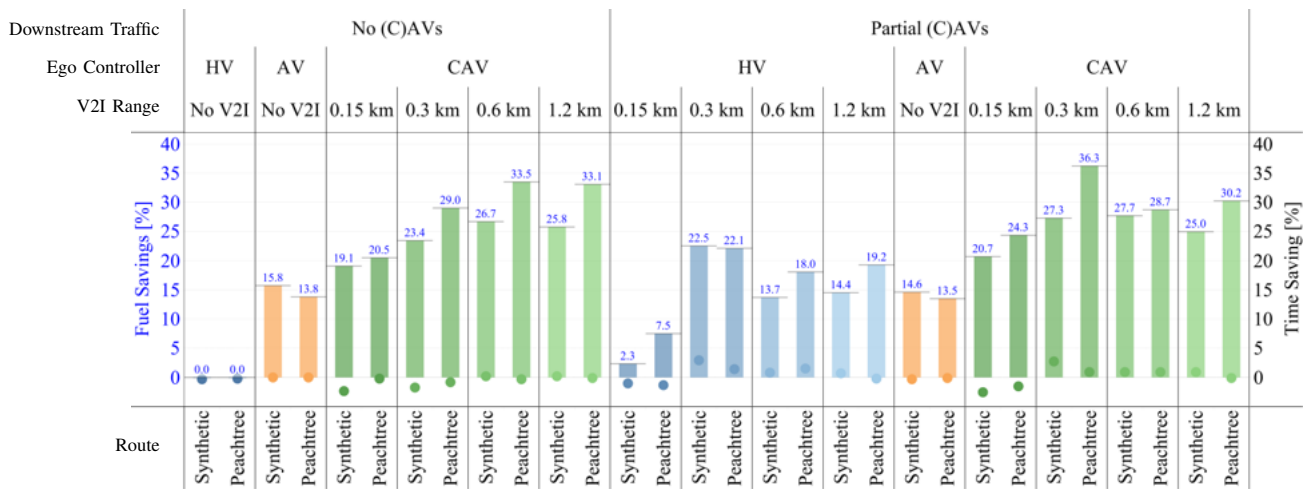


Fig. 10: Measured energy (bar) and time (dot) performance of the ego vehicle control approaches compared to HV as baseline.

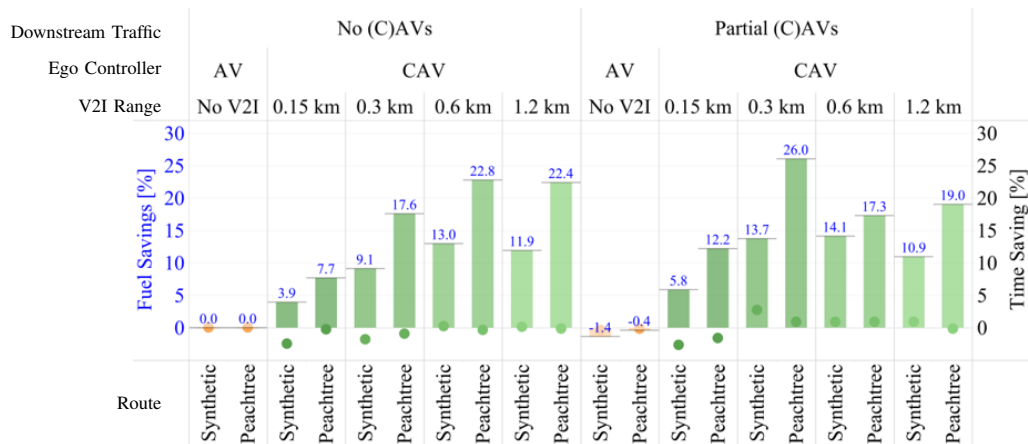


Fig. 11: Measured energy (bar) and time (dot) performance of the ego vehicle control approaches compared to AV as baseline.

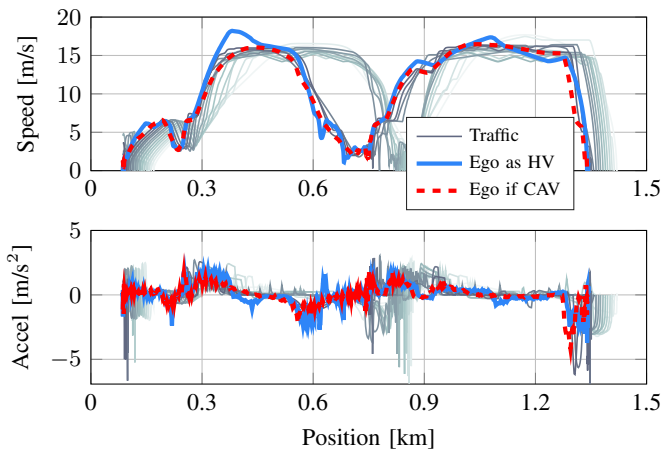
compared to if the ego CAV has a long connectivity range, it achieves strong fuel performance regardless of the presence of downstream CAVs.

#### A. Effects on Human Drivers

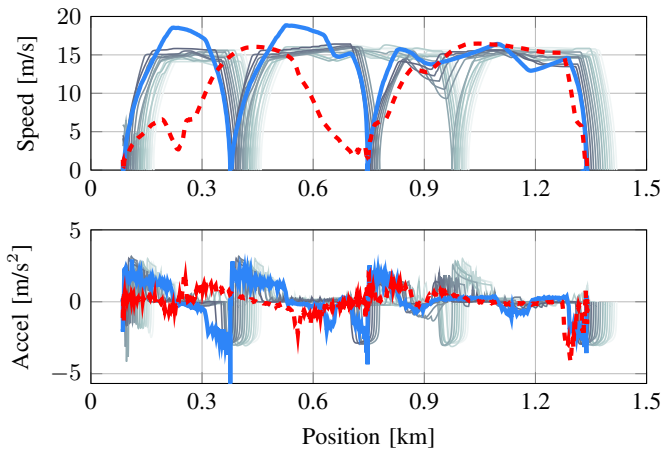
Next, it should be noted that the smooth driving of CAVs can extend significant benefits to surrounding traffic by creating a positive impedance that encourages them to drive at more eco-friendly speeds. This is particularly demonstrated in Figure 12, which contrasts the velocity and acceleration profiles of the ego HV when driving in the case with partial CAVs downstream to the case with no CAVs present. Overlaid over both profiles is the realized trajectories as if the ego vehicle was driven as a CAV: it can be seen that the HV itself followed the general shape of the optimal profile by driving behind CAVs. Overall, it is important for drivers to drive near the optimal eco-speeds, however deviation can be tolerated to still realize significant fuel benefits. As can be seen in Figure 10, the ego HV performed with up to 22% fuel economy improvement in partial CAV scenarios. This result further depends on available connectivity range: when connectivity range is too limited, as in the 0.15 km case, fuel savings in the ego HV are limited between 2-7%. However,

the fuel economy of the ego HV improved between 14-22% with increasing connectivity ranges up to 1.2 km. This study currently examines these positive benefits on surrounding traffic for single-lane scenarios, and so later studies should consider traffic impacts due to CAVs in multi-lane scenarios.

Finally, the fuel performance of each microsimulated vehicle is additionally estimated. Vehicle fuel and emissions estimation software Autonomie is used to trace the microsimulated drive cycles from traffic using a mid-size SUV combustion powertrain [39]. Figure 13 depicts the estimated fuel performance of each microsimulated vehicle for the Synthetic and Peachtree routes. Here, the fuel economy improvement for each of the 13 simulated vehicles is reported with respect to its corresponding performance in the scenario with all human drivers in the fleet. Vehicle ID 1 corresponds to the leader vehicle in the string, and vehicles 1 and 11 were the designated (C)AVs during experimentation when considering the partial CAVs case. Other vehicles were designated as simulated HVs in all scenarios. It can be seen that positive fuel improvements to human drivers were concentrated to those vehicles driving more immediately behind a CAV, and in some measured cases provided significant fuel improvements of up to 80%. It should be noted that the string fuel performance was largely



(a) Scenario with downstream CAVs (1200 m range).



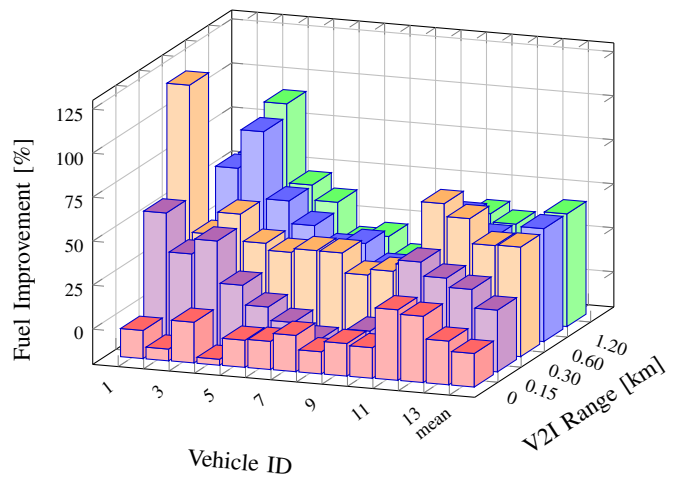
(b) Scenario without downstream CAVs.

Fig. 12: Performance trajectories of the ego when operated as an HV. Overlaid is the vehicle trajectory if operated as a CAV. Downstream traffic is shown in black, with darker shades representing vehicles closer to the ego.

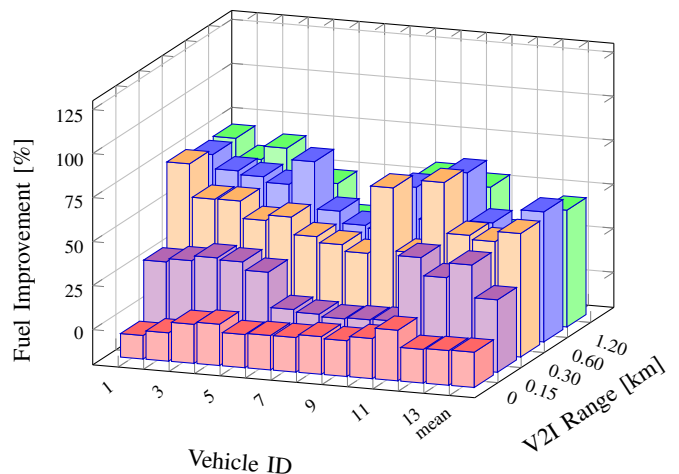
unaffected in the 0 m V2I range case (mean fuel economies were within 1% of the baseline), and that drivers 7-9 had either neutral fuel performance in the Peachtree route or *worsened* fuel performance by up to 10% in the Synthetic route when V2I range was limited to 150 m. Importantly, increasing V2I connectivity range had a positive fuel efficiency trend. Overall for each route, the mean fuel economy improvement of the average vehicle in the string increased between 40-50% when connectivity range was at least 300 m.

### B. Future Work

In a system without noise or disturbances, we expect that increasing connectivity range in the CAVs will monotonically increase fuel economy. Experimentally, with traffic included in the testing scenarios, this trend was observed to be generally true except the outlier 0.3 km cases performed the best. Traffic disrupts the planned acceleration-optimal trajectories, which become more forward-looking with higher connectivity ranges that can conversely become more sensitive to traffic



(a) Synthetic route.



(b) Peachtree route.

Fig. 13: Autonomie estimated fuel improvements of each simulated vehicle in the partial CAVs case with respect to its performance in the all-human scenario [39]. Here, vehicle IDs 1 and 11 are automated.

impacts. The eco-speed planner of Section II assumes free-flow conditions and adjusts intersection entering times with margin parameters ( $\delta t_{des}$ ,  $\delta t_{fea}$ ). In future work, assessing traffic inhibition and queueing effects in the speed planning stage would further improve fuel economy and provide more consistently beneficial results. Additionally, the speed planner may further benefit from directly penalizing fuel consumption of the ego vehicle, and future work could investigate performance differences between the acceleration penalty and a fuel penalty. Additionally, if considering multiple lanes in an urban corridor, surrounding traffic has the opportunity to overtake the (perceivingly) slow-moving CAVs, thereby negating some of the positive energy improvements forced by driving in an energy-efficient speed profile upstream of a CAV. Multi-lane corridors are to be considered in future work.

## VI. CONCLUSION

The performance of eco-driving in urban corridors was presented through experimentation of a prototype connected and automated vehicle. Said eco-driving was informed by preview of upcoming SPaT as made available through V2I-connected communication with downstream traffic intersections. Eco-driving was posed as a bi-level optimization problem, in which the solutions to an inner, sub-optimization problem form the constraints on decision variables of an outer optimization. Pontryagin's Minimum Principle was utilized to derive algebraic expressions for the solution to the sub-problem: which lead to efficient, real-time compatible numerical solutions to the overall optimal control problem. Travel time was explicitly enforced as a boundary condition in the optimal control problem, and travel time differences of all trials were within 5 s of each other.

The prototype CAV was experimentally vetted through a vehicle-in-the-loop procedure, which allowed for efficiently and quickly testing in a variety of scenarios by simulating the nearby traffic scene. The fuel and travel time performance of the ego experimental vehicle was studied when varying: downstream traffic composition between all HVs and a mixture of HVs and CAVs, available connectivity range, and route that affected placement and timing of traffic lights. Several control strategies that considered the ego vehicle as a human driver, automated driver with no SPaT preview, and a connected and automated driver with SPaT preview were considered. Overall, between 19-36% fuel savings were measured with the proposed control approach over the human-modelled driver.

Additionally, automation itself provides an opportunity to improve fuel economy by enforcing smooth driving and reducing unnecessary braking: between 13-15% fuel savings were measured when using an automated vehicle strategy that was not V2I-connected.

Downstream traffic patterns also have a role in measured fuel economy of the ego vehicle by affecting its motion. When the ego vehicle was operated as a human driver but there were V2I-connected CAVs downstream, eco-driving benefits were extended to the human driver and 14-22% fuel savings were measured over the CAV-less scenario. Autonomie simulation was conducted to estimate the network-wide fuel usage of the simulated vehicles downstream. Energy performance of individual human drivers when driving in an all-human scenario compared to a scenario with 15% CAVs improved by 50% on average with a connectivity range of at least 300 m. When driving in a scenario with AVs not equipped with connectivity, human drivers did not realize an average benefit in energy economy. Such findings suggest the potential for significant fuel savings at a network-wide level with the introduction of partial CAVs, and the critical importance that connectivity technology has on realizing said benefits.

### APPENDIX A

#### MULTI-POINT BOUNDARY VALUE PROBLEM

The control Hamiltonian for a dynamical system  $f(x, u)$  that minimizes a performance index  $J = \int_0^T L(x, u) dt$  is given as  $H = L + \lambda^T f$  - and for inner OCP (7) is further

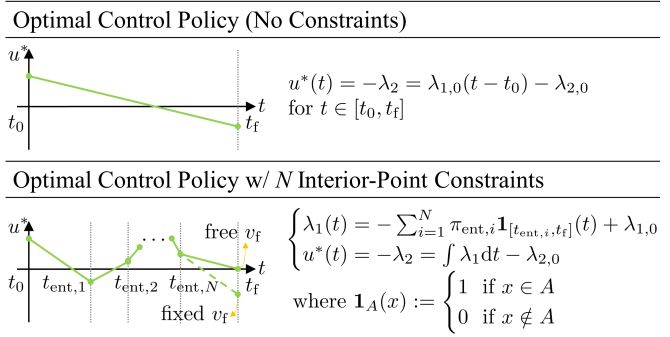


Fig. 14: Summary of the optimal control policy depending on whether interior-point constraints exist.

$H = 1/2 u^2 + \lambda_1 x_2 + \lambda_2 u$ , with  $\lambda_1$  and  $\lambda_2$  as the position and speed co-states, respectively [37].

Deploying Pontryagin's Minimum Principle, the inner OCPs in Eq. (7) can be transformed into a boundary value problem (BVP), and where the interior-point constraints result in a multi-point BVP. The resulting ordinary differential equation is expressed as

$$\begin{aligned} \frac{d}{dt} [s^*, v^*, \lambda_1, \lambda_2]^T &= [v^*, -\lambda_2, 0, -\lambda_1]^T \\ \text{with } \lambda_1(t_{ent,i}^-) &= \lambda_1(t_{ent,i}^+) + \pi_{ent,i} \text{ for } i = 1 \dots N, \end{aligned}$$

where  $\pi_{ent,i}$  is a jump parameter, which leads to an optimal control policy that is piece-wise linear, as illustrated in Figure 14. The boundary values at  $(N + 2)$  points are

$$\begin{cases} s(t_0) = s_0 \text{ and } v(t_0) = v_0, \\ s(t_{ent,i}) = s_i \text{ for } i = 1 \dots N, \\ s(t_f) = s_f \text{ and } \begin{cases} v(t_f) = v_f & \text{if } v(t_f) \text{ is fixed} \\ \lambda_2(t_f) = \lambda_{2,f} = 0 & \text{if } v(t_f) \text{ is free.} \end{cases} \end{cases}$$

We obtain a system of  $(N + 2)$  nonlinear equations satisfying the  $(N + 2)$ -point boundary conditions in  $(N + 2)$  unknowns (such as  $\pi_{ent,i}$  for  $i = 1 \dots N + 1$  and two initial values of  $\lambda_1$  and  $\lambda_2$ ).

### APPENDIX B

#### SERIES OF TWO-POINT BOUNDARY VALUE PROBLEMS

For further simplicity of computation, the multi-point BVP can then be converted to a series of two-point BVPs (TP-BVPs) in each sub-interval between points that search intersection entering-speeds and ensure the continuity of the  $\lambda_2$  variable. The  $i$ -th TP-BVP is defined as a function of  $(v_{i-1}, v_i, l_i, \xi_i)$ , where  $\xi_i = t_{f,i} - t_{0,i}$ . As the optimal control policy is a linear function in time for the  $i$ -th TP-BVP (shown in Figure 14), boundary values of the  $\lambda$  variables at the two points are expressed as

$$\begin{cases} \lambda_1(t_{0,i}^+) = \lambda_{1,i-1}^+ = -12l_i \xi_i^{-3} + 6(v_{i-1} + v_i) \xi_i^{-2}, \\ \lambda_2(t_{0,i}^+) = \lambda_{2,i-1}^+ = -6l_i \xi_i^{-2} + 2(2v_{i-1} + v_i) \xi_i^{-1}, \\ \lambda_1(t_{f,i}^-) = \lambda_{1,i}^- = \lambda_{1,i-1}^+, \\ \lambda_2(t_{f,i}^-) = \lambda_{2,i}^- = 6l_i \xi_i^{-2} - 2(v_{i-1} + 2v_i) \xi_i^{-1}. \end{cases}$$

The  $i$ -th continuity condition for  $\lambda_2$  is imposed by the final value of the  $i$ -th TP-BVP and the initial value of the  $(i+1)$ -th TP-BVP, as

$$\lambda_{2,i}^- = \lambda_{2,i}^+ \text{ for } i = 1 \dots N.$$

In such a way, the original system of  $(N+2)$  nonlinear equations can be transformed into the system of  $N$  linear equations satisfying  $N$  continuity conditions at  $t_{\text{ent},i}$  in  $N$  unknowns (such as  $v_i$  for  $i = 1 \dots N$ ), as

$$\begin{bmatrix} y_1 - 2v_0\xi_1^{-1} \\ y_2 \\ \vdots \\ y_{N-1} \\ y_N - k_0 \end{bmatrix}_{\mathbf{y} \in \mathbb{R}^N} = \begin{bmatrix} a_1 & b_1 & 0 & \cdots & 0 \\ b_1 & a_2 & b_2 & \cdots & 0 \\ 0 & b_2 & a_3 & \ddots & 0 \\ \vdots & \vdots & \vdots & \ddots & \vdots \\ 0 & 0 & \ddots & \ddots & b_{N-1} \\ 0 & 0 & 0 & b_{N-1} & a_N - k_1 \end{bmatrix}_{\mathbf{A} \in \mathbb{R}^{N \times N}} \begin{bmatrix} v_1^* \\ v_2^* \\ \vdots \\ v_{N-1}^* \\ v_N^* \end{bmatrix}_{\mathbf{v}^* \in \mathbb{R}^N}$$

where  $A$  is a symmetric tridiagonal matrix with  $a_i = 4(\xi_i^{-1} + \xi_{i+1}^{-1})$ ,  $b_i = 2\xi_{i+1}^{-1}$ ,  $y_i = 6l_i\xi_i^{-2} + 6l_{i+1}\xi_{i+1}^{-2}$ , and

$$\begin{cases} (k_0, k_1) = (2v_f\xi_1^{-1}, 0) & \text{if } v(t_f) \text{ is fixed} \\ (k_0, k_1) = (3l_{N+1}\xi_{N+1}^{-2}, \xi_{N+1}^{-1}) & \text{if } v(t_f) \text{ is free.} \end{cases}$$

#### DISCLAIMER

The submitted manuscript has been created in part by UChicago Argonne, LLC, Operator of Argonne National Laboratory (“Argonne”). Argonne, a U.S. Department of Energy Office of Science laboratory, is operated under Contract No. DE-AC02-06CH11357. The U.S. Government retains for itself, and others acting on its behalf, a paid-up nonexclusive, irrevocable worldwide license in said article to reproduce, prepare derivative works, distribute copies to the public, and perform publicly and display publicly, by or on behalf of the Government. The Department of Energy (DOE) will provide public access to these results of federally sponsored research in accordance with the DOE Public Access Plan.

#### ACKNOWLEDGMENT

The authors would like to thank Mr. Rongyao (Tony) Wang, Mr. Viranjan Bhattacharrya, and Mr. Prakhar Gupta in their assistance in conducting vehicle experiments.

This report and the work described were sponsored by the U.S. Department of Energy (DOE) Vehicle Technologies Office (VTO) under the Systems and Modeling for Accelerated Research in Transportation (SMART) Mobility Laboratory Consortium, an initiative of the Energy Efficient Mobility Systems (EEMS) Program.

The following DOE Office of Energy Efficiency and Renewable Energy (EERE) managers played important roles in establishing the project concept, advancing implementation, and providing ongoing guidance: Prasad Gupte, Jacob Ward, Heather Croteau, and David Anderson.

#### REFERENCES

- [1] A. Vahidi and A. Sciarretta, “Energy saving potentials of connected and automated vehicles,” *Transportation Research Part C: Emerging Technologies*, vol. 95, no. April 2018, pp. 822–843, 2018. [Online]. Available: <https://doi.org/10.1016/j.trc.2018.09.001>
- [2] J. Guanetti, Y. Kim, and F. Borrelli, “Control of connected and automated vehicles: State of the art and future challenges,” *Annual Reviews in Control*, vol. 45, no. May, pp. 18–40, 2018. [Online]. Available: <https://doi.org/10.1016/j.arcontrol.2018.04.011>
- [3] Z. Wang, Y. Bian, S. E. Shladover, G. Wu, S. E. Li, and M. J. Barth, “A Survey on Cooperative Longitudinal Motion Control of Multiple Connected and Automated Vehicles,” *IEEE Intelligent Transportation Systems Magazine*, vol. 12, no. 1, pp. 4–24, 2020.
- [4] R. Sarkar and J. Ward, *DOE SMART Mobility: Systems and Modeling for Accelerated Research in Transportation*. Cham: Springer International Publishing, 2016, pp. 39–52. [Online]. Available: [https://doi.org/10.1007/978-3-319-40503-2\\_4](https://doi.org/10.1007/978-3-319-40503-2_4)
- [5] S. E. Shladover, C. Nowakowski, X.-Y. Lu, and R. Ferlis, “Cooperative adaptive cruise control: Definitions and operating concepts,” *Transportation Research Record*, vol. 2489, 2015.
- [6] B. Asadi and A. Vahidi, “Predictive cruise control: Utilizing upcoming traffic signal information for improving fuel economy and reducing trip time,” *IEEE Transactions on Control Systems Technology*, vol. 19, no. 3, pp. 707–714, 2011.
- [7] A. Talebpour and H. S. Mahmassani, “Influence of connected and autonomous vehicles on traffic flow stability and throughput,” *Transportation Research Part C: Emerging Technologies*, vol. 71, no. July, pp. 143–163, 2016. [Online]. Available: <http://dx.doi.org/10.1016/j.trc.2016.07.007>
- [8] J. Rios-Torres and A. A. Malikopoulos, “Impact of Partial Penetrations of Connected and Automated Vehicles on Fuel Consumption and Traffic Flow,” *IEEE Transactions on Intelligent Vehicles*, vol. 3, no. 4, pp. 453–462, 2018.
- [9] T. Ard, R. A. Dollar, A. Vahidi, Y. Zhang, and D. Karbowski, “Microsimulation of energy and flow effects from optimal automated driving in mixed traffic,” *Transportation Research Part C: Emerging Technologies*, vol. 120, p. 102806, 2020. [Online]. Available: <https://www.sciencedirect.com/science/article/pii/S0968090X20307130>
- [10] H. Liu, S. E. Shladover, X. Y. Lu, and X. Kan, “Freeway vehicle fuel efficiency improvement via cooperative adaptive cruise control,” *Journal of Intelligent Transportation Systems: Technology, Planning, and Operations*, vol. 0, no. 0, pp. 1–13, 2020.
- [11] V. Jayawardana and C. Wu, “Learning eco-driving strategies at signalized intersections,” in *European Control Conference (ECC)*, 2022.
- [12] N. Wan, A. Vahidi, and A. Luckow, “Optimal speed advisory for connected vehicles in arterial roads and the impact on mixed traffic,” *Transportation Research Part C: Emerging Technologies*, vol. 69, pp. 548–563, 2016. [Online]. Available: <https://www.sciencedirect.com/science/article/pii/S0968090X16000292>
- [13] H. Yang, H. Rakha, and M. V. Ala, “Eco-cooperative adaptive cruise control at signalized intersections considering queue effects,” *IEEE Transactions on Intelligent Transportation Systems*, vol. 18, no. 6, pp. 1575–1585, 2017.
- [14] J. I. Ge, S. S. Avedisov, C. R. He, W. B. Qin, M. Sadeghpour, and G. Orosz, “Experimental validation of connected automated vehicle design among human-driven vehicles,” *Transportation Research Part C: Emerging Technologies*, vol. 91, no. April, pp. 335–352, 2018. [Online]. Available: <https://doi.org/10.1016/j.trc.2018.04.005>
- [15] S. S. Avedisov, G. Bansal, and G. Orosz, “Impacts of connected automated vehicles on freeway traffic patterns at different penetration levels,” *IEEE Transactions on Intelligent Transportation Systems*, vol. 23, no. 5, pp. 4305–4318, 2022.
- [16] A. Ibrahim, M. Cicic, D. Goswami, T. Basten, and K. H. Johansson, “Control of Platooned Vehicles in Presence of Traffic Shock Waves,” *2019 IEEE Intelligent Transportation Systems Conference, ITSC 2019*, pp. 1727–1734, 2019.
- [17] G. Mahler, A. Winckler, S. A. Fayazi, M. Filusch, and A. Vahidi, “Cellular communication of traffic signal state to connected vehicles for arterial eco-driving,” in *2017 IEEE 20th International Conference on Intelligent Transportation Systems (ITSC)*, 2017, pp. 1–6.
- [18] H. Chen and H. A. Rakha, “Developing and field testing a green light optimal speed advisory system for buses,” *Energies*, vol. 15, no. 4, 2022. [Online]. Available: <https://www.mdpi.com/1996-1073/15/4/1491>
- [19] M. Kamal, M. Mukai, J. Murata, and T. Kawabe, “Ecological driving based on preceding vehicle prediction using MPC,” *IFAC Proceedings Volumes*, vol. 44, no. 1, pp. 3843–3848, 2011, 18th IFAC World Congress. [Online]. Available: <https://www.sciencedirect.com/science/article/pii/S1474667016442102>
- [20] M. A. S. Kamal, M. Mukai, J. Murata, and T. Kawabe, “Model predictive control of vehicles on urban roads for improved fuel economy,” *IEEE Transactions on Control Systems Technology*, vol. 21, no. 3, pp. 831–841, 2013.

- [21] Z. Wang, G. Wu, and M. J. Barth, "Cooperative eco-driving at signalized intersections in a partially connected and automated vehicle environment," *IEEE Transactions on Intelligent Transportation Systems*, vol. 21, no. 5, pp. 2029–2038, 2020.
- [22] B. HomChaudhuri, A. Vahidi, and P. Pisu, "Fast Model Predictive Control-Based Fuel Efficient Control Strategy for a Group of Connected Vehicles in Urban Road Conditions," *IEEE Transactions on Control Systems Technology*, vol. 25, no. 2, pp. 760–767, 2017.
- [23] Y. J. Zhang, A. A. Malikopoulos, and C. G. Cassandras, "Optimal control and coordination of connected and automated vehicles at urban traffic intersections," *Proceedings of the American Control Conference*, vol. 2016-July, pp. 6227–6232, 2016.
- [24] A. A. Malikopoulos, C. G. Cassandras, and Y. J. Zhang, "A decentralized energy-optimal control framework for connected automated vehicles at signal-free intersections," *Automatica*, vol. 93, pp. 244–256, 2018. [Online]. Available: <https://doi.org/10.1016/j.automatica.2018.03.056>
- [25] G. Mahler and A. Vahidi, "An optimal velocity-planning scheme for vehicle energy efficiency through probabilistic prediction of traffic-signal timing," *IEEE Transactions on Intelligent Transportation Systems*, vol. 15, no. 6, pp. 2516–2523, 2014.
- [26] C. Sun, J. Guanetti, F. Borrelli, and S. J. Moura, "Optimal Eco-Driving Control of Connected and Autonomous Vehicles Through Signalized Intersections," *IEEE Internet of Things Journal*, vol. 7, no. 5, pp. 3759–3773, 2020.
- [27] K. Dresner and P. Stone, "A Multiagent Approach to Autonomous Intersection Management," *Journal of Artificial Intelligence Research*, 2008.
- [28] M. Quinlan, T. C. Au, J. Zhu, N. Sturca, and P. Stone, "Bringing simulation to life: A mixed reality autonomous intersection," *IEEE/RSJ 2010 International Conference on Intelligent Robots and Systems, IROS 2010 - Conference Proceedings*, no. October, pp. 6083–6088, 2010.
- [29] S. A. Fayazi and A. Vahidi, "Vehicle-in-the-loop (vil) verification of a smart city intersection control scheme for autonomous vehicles," in *2017 IEEE Conference on Control Technology and Applications (CCTA)*, 2017, pp. 1575–1580.
- [30] A. M. I. Mahbub, V. Karri, D. Parikh, S. Jade, and A. A. Malikopoulos, "A decentralized time- and energy-optimal control framework for connected automated vehicles: From simulation to field test," in *SAE Technical Paper*. SAE International, 04 2020. [Online]. Available: <https://doi.org/10.4271/2020-01-0579>
- [31] Y. Feng, C. Yu, S. Xu, H. X. Liu, and H. Peng, "An augmented reality environment for connected and automated vehicle testing and evaluation," in *2018 IEEE Intelligent Vehicles Symposium (IV)*, 2018, pp. 1549–1554.
- [32] T. Ard, L. Guo, R. A. Dollar, A. Fayazi, N. Goulet, Y. Jia, B. Ayalew, and A. Vahidi, "Energy and flow effects of optimal automated driving in mixed traffic: Vehicle-in-the-loop experimental results," *Transportation Research Part C: Emerging Technologies*, vol. 130, p. 103168, 2021. [Online]. Available: <https://www.sciencedirect.com/science/article/pii/S0968090X21001868>
- [33] H. Xia, K. Boriboonsomsin, F. Schweizer, A. Winckler, K. Zhou, W.-B. Zhang, and M. Barth, "Field operational testing of eco-approach technology at a fixed-time signalized intersection," in *2012 15th International IEEE Conference on Intelligent Transportation Systems*, 2012, pp. 188–193.
- [34] M. H. Almannaa, H. Chen, H. A. Rakha, A. Loulizi, and I. El-Shawarby, "Field implementation and testing of an automated eco-cooperative adaptive cruise control system in the vicinity of signalized intersections," *Transportation Research Part D: Transport and Environment*, vol. 67, pp. 244–262, 2019. [Online]. Available: <https://www.sciencedirect.com/science/article/pii/S1361920918305583>
- [35] S. Bae, Y. Kim, Y. Choi, J. Guanetti, P. Gill, F. Borrelli, and S. J. Moura, "Ecological adaptive cruise control of plug-in hybrid electric vehicle with connected infrastructure and on-road experiments," *Journal of Dynamic Systems, Measurement, and Control*, vol. 144, no. 1, 01 2022, 011109. [Online]. Available: <https://doi.org/10.1115/1.4053187>
- [36] J. Han, D. Shen, D. Karbowski, and A. Rousseau, "Leveraging multiple connected traffic light signals in an energy-efficient speed planner," *IEEE Control Systems Letters*, vol. 5, no. 6, pp. 2078–2083, 2021.
- [37] A. E. Bryson and Y. Ho, *Applied optimal control: optimization, estimation, and control*. CRC Press, 1975.
- [38] PTV Group, *PTV VISSIM 10 User Manual*. PTV AG, 2018.
- [39] S. Halbach, P. Sharer, S. Pagerit, C. Folkerts, and A. Rousseau, "Model architecture, methods, and interfaces for efficient math-based design and simulation of automotive control systems," 04 2010.



**Tyler Ard** Tyler Ard received the B.Sc. degree in mechanical engineering from Clemson University in 2017. He is currently a candidate for the Ph.D. degree in mechanical engineering from Clemson University, where his research includes developing and verifying eco-driving strategies for ADAS and autonomous driving systems - in the aim of more efficient energy utilization of technologies already available today.



**Longxiang Guo** Longxiang Guo (S'17-M'21) received the B.Sc. degree in mechanical engineering from Tsinghua University, Beijing, China, in 2012, the M.Sc. degree in mechanical engineering from Chinese Academy of Sciences, Shenzhen, China, in 2015, and the Ph.D. degree in automotive engineering from Clemson University in 2021. Currently, he is working as a postdoctoral fellow at Clemson University International Center for Automotive Research (CU-ICAR).



**Jihun Han** Jihun Han received his B.Sc., M.Sc., and Ph.D. in Mechanical Engineering from Korea Advanced Institute of Science and Technology (KAIST), South Korea, in 2009, 2011 and 2016, respectively. He was a postdoctoral research associate at IFP Energies Nouvelles, France, in 2016-2017, and at Oak Ridge National Laboratory, USA, in 2017-2018. He is currently a principal research engineer at the Vehicle and Mobility Simulation group and has worked at Argonne National Laboratory since 2018. His research interests include modeling,

control, and simulation with an emphasis in intelligent transportation systems, and connected and automated vehicle systems.



**Yunyi Jia** Yunyi Jia (S'08-M'15-SM'20) received the B.Sc. degree from National University of Defense Technology, M.Sc. degree from South China University of Technology and Ph.D. degree from Michigan State University. He is currently the McQueen Quattlebaum Associate Professor and the director of Collaborative Robotics and Automation (CRA) Lab in the Department of Automotive Engineering at Clemson University International Center for Automotive Research. His research interests include collaborative robotics, automated vehicles and

advanced sensing systems.



**Ardalan Vahidi** Ardalan Vahidi (Senior Member, IEEE) received the B.Sc. and M.Sc. degrees in civil engineering from the Sharif University of Technology, Tehran, Iran, in 1996 and 1998, respectively, the M.Sc. degree in transportation safety from George Washington University, Washington, DC, USA, in 2002, and the Ph.D. degree in mechanical engineering from the University of Michigan, Ann Arbor, MI, USA, in 2005. From 2012 to 2013, he was a Visiting Scholar with the University of California at Berkeley, Berkeley, CA, USA. He has held scientific

visiting positions at the BMW Technology Office, Mountain View, CA, USA, and IFP Energies Nouvelles, Rueil-Malmaison, France. He is currently Professor of Mechanical Engineering with Clemson University, Clemson, SC, USA. His recent publications span topics connected and autonomous vehicles, efficient transportation, and human performance. He is a Fellow of ASME.



**Dominik Karbowski** Dominik Karbowski is the Manager of the Intelligent Vehicle Controls and Low-Carbon Aviation Team, within the Vehicle and Mobility Simulation Group at Argonne National Laboratory. He leads Argonne's effort to improve vehicle energy efficiency through control, data science, connectivity and automation, and using advanced systems simulation research. His research interests include: energy-focused controls for Connected and Automated Vehicles (CAVs), intelligent energy management and powertrain control, driver behavior,

real-world driving data analytics, advanced powertrains, aircraft systems optimization. He is a major developer of simulation tools for transportation energy-efficient vehicle research. He has made significant contributions to Autonomie, Argonne's road vehicle energy consumption tool, and has invented several software to support his research such as SVTRP, RoadRunner, and Aeronomie. He holds a master of science in engineering from Mines Paris - PSL in France.